Exploring the molecular biology of ischemic cardiomyopathy based on ferroptosis-related genes

SHI-TAO ZHAO[1,2*], ZHI-CONG QIU[1,2*], RUI-YUAN ZENG[1,2*], HUA-XI ZOU[3], RONG-BIN QIU[1,2], HAN-ZHI PENG[1,2], LIAN-FEN ZHOU[1,2], ZHI-QIANG XU[1,2], SONG-QING LAI[1,2] and LI WAN[1,2]

[1]Department of Cardiovascular Surgery and [2]Institute of Cardiovascular Surgical Diseases, The First Affiliated Hospital, Jiangxi Medical College, Nanchang University, Nanchang, Jiangxi 330006; [3]Department of Cardiovascular Surgery, The Second Affiliated Hospita, Jiangxi Medical College, Nanchang University, Nanchang, Jiangxi 330200, P.R. China

Received October 5, 2023; Accepted February 21, 2024

DOI: 10.3892/etm.2024.12509

Abstract. Ischemic cardiomyopathy (ICM) is a serious cardiac disease with a very high mortality rate worldwide, which causes myocardial ischemia and hypoxia as the main damage. Further understanding of the underlying pathological processes of cardiomyocyte injury is key to the development of cardioprotective strategies. Ferroptosis is an iron-dependent form of regulated cell death characterized by the accumulation of lipid hydroperoxides to lethal levels, resulting in oxidative damage to the cell membrane. The current understanding of the role and regulation of ferroptosis in ICM is still limited, especially in the absence of evidence from large-scale transcriptomic data. Through comprehensive bioinformatics analysis of human ICM transcriptome data obtained from the Gene Expression Omnibus database, the present study identified differentially expressed ferroptosis-related genes (DEFRGs) in ICM. Subsequently, their potential biological mechanisms and cross-talk were analyzed, and hub genes were identified by constructing protein-protein interaction networks. Ferroptosis features such as reactive oxygen species generation, changes in ferroptosis marker proteins, iron ion aggregation and lipid oxidation, were identified in the H9c2 anoxic reoxygenation injury model. Finally, the diagnostic ability of Gap junction alpha-1 (GJA1), Solute carrier family 40 member 1 (SLC40A1), Alpha-synuclein (SNCA) were identified through receiver operating characteristic curves and the expression of DEFRGs was verified in an *in vitro* model. Furthermore, potential drugs (retinoic acid) that could regulate ICM ferroptosis were predicted based on key DEFRGs. The present article presents new insights into the role of ferroptosis in ICM, investigating the regulatory role of ferroptosis in the pathological process of ICM and advocating for ferroptosis as a potential novel therapeutic target for ICM based on evidence from the ICM transcriptome.

Correspondence to: Professor Li Wan or Dr Song-Qing Lai, Department of Cardiovascular Surgery, The First Affiliated Hospital, Jiangxi Medical College, Nanchang University, 17 Yongwai Zheng Road, Donghu, Nanchang, Jiangxi 330006, P.R. China
E-mail: ndyfy02131@ncu.edu.cn
E-mail: ndyfy03743@ncu.edu.cn

*Contributed equally

Key words: ischemic cardiomyopathy, ferroptosis, heart transcriptome, bioinformatics, database

Introduction

Ischemic cardiomyopathy (ICM) is one of the most common cardiomyopathies with a high rate of sudden cardiac death; >9 million people suffering from chronic stable angina in the United States alone (1). It is characterized by several clinical manifestations which manifest clinically as dyspnea or chest pain, and has a pathophysiological basis in myocardial ischemia and hypoxia due to coronary atherosclerosis, as well as myocardial cell reduction, necrosis, myocardial fibrosis and myocardial scar formation (2,3). Advances in medical technology have made it possible to treat ICM with a range of clinical treatments, including drugs, thrombus recanalization, stent implantation and cardiac bypass surgery (4). Restoring blood flow after ischemia remains the best therapeutic option in limiting myocardial infarct size and maintaining cardiac function (5). However, it can also trigger adverse effects that damage myocardium known as ischemia/reperfusion (I/R) injury (6). The pathogenesis of ICM is complex and there is a lack of a definitive clinical management strategy (7). Current therapeutic strategies to prevent myocardial I/R injury are helping to treat ICM (8). Therefore, it is crucial to clarify the molecular biological mechanisms of ischemic cardiomyopathy as well as new therapeutic strategies.

Ferroptosis is an iron-dependent form of regulated cell death (9). Ferroptosis causes oxidative damage to cell membranes, through the continuous accumulation of lipid hydroperoxides (10). Studies have reported that most diseases are associated with ferroptosis, such as cancer (11), traumatic brain injury (12), intracerebral hemorrhage (13) and I/R injury (14), and ferroptosis is an important form of myocardial cell death in myocardial I/R injury (15). In clinical practice, patients with myocardial infarction (MI) often experience left ventricular remodeling accompanied by the accumulation

of ferrous ions, and large amounts of ferrous ions have been reported in the infarcted tissue of patients with ST-segment elevation MI (16). Moreover, iron overload may cause cardiomyocyte death, which is an important mechanism in the development of cardiomyopathy (17). Investigating the molecular mechanism of ferroptosis in I/R injury and understanding the potential therapeutic targets related to ferroptosis may effectively reduce myocardial I/R injury and avoid the advancement of ICM during treatment.

In the present study, a systematic bioinformatics analysis was performed to analyze the differential expression of ferroptosis-related genes (FRGs) in ICM and their potential crosstalk and functional pathways, which contributes to an in-depth understanding of the mechanisms and new diagnostic and therapeutic targets in ICM. A protein-protein interaction (PPI) network was constructed to identify the hub genes. Subsequently, the expression of hub genes and ferroptosis characteristics were verified in the H9c2 anoxic reoxygenation (A/R) injury model, and then the diagnostic ability of hub genes for ICM was evaluated. Finally, potential ferroptosis-regulating drugs were predicted for ICM based on key genes in the Drug Signatures Database (DSigDB), which will help to improve the likelihood of translating the drugs into the clinic.

Materials and methods

Data collection. The microarray datasets GSE26887 (18) and GSE57338 (19) were retrieved from the Gene Expression Omnibus (GEO) database (https://www.ncbi.nlm.nih.gov/geo/) (20). In the present study, data from 12 post-ischemic myocardium samples and 5 non-heart failure heart-matched donor heart samples from the GSE26887 dataset were subjected to RNA sequencing analysis and bioinformatic exploration. For validation, data from 94 post-ischemic myocardium samples and 137 non-heart failure heart-matched donor heart samples from the GSE57338 dataset were used.

Gene set enrichment analysis (GSEA). GSEA was performed using GSEA software (v4.2.3) (http://software.broadinstitute.org/gsea/index.jsp) (21) to observe the overall correlation between ferroptosis and ICM. Genes in the GSE26887 dataset were scored using the ferroptosis custom dataset in GSEA. The normalized enrichment score (NES) was calculated and P.adjust <0.05 was considered to indicate a statistically significant difference.

Weighted gene co-expression network analysis (WGCNA) in GSE26887. The 'WGCNA' R package (v1.72-1) (22) was used and WGCNA was performed on GSE26887, with abnormal samples removed to ensure reliable results of the network construction. Firstly, an optimal soft threshold was set to divide the data into different modules by the 'flashClust' (v1.01-2-3) (22) function in WGCNA. The adjacency matrix consisted of continuous values between 0-1, thus the constructed network conformed to a power-law distribution and represented the real biological state more accurately. Secondly, the block module function was used to construct scale-free networks and perform module partitioning analysis. Each module was summarized by module identity genes, and each module was illustrated in color. Ultimately, the module which demonstrated the highest positive correlation with the ICM was identified.

Identification of differentially expressed genes (DEGs) and differentially expressed FRGs (DEFRGs). The 'limma' R package (v3.52.0) (23) was used to determine the DEGs between ICM and normal hearts. The thresholds set for selecting the DEGs were $\log_2$fold change (FC) ≥0.50 and false discovery rate (FDR) <0.05. The volcanoes and heat maps of the DEGs were plotted using the 'ggplot2' R package (v3.4.3) (24). A total of 484 FRGs were acquired from the FerrDb database (http://www.zhounan.org/ferrdb/) (25), classified as Driver, Suppressor and Marker genes (Table SI). The online Venn diagram tool (v1.9.0) (https://jvenn.toulouse.inrae.fr/app/example.html) (26) overlapped the most ICM-correlated modular genes, DEGs in GSE26887 and FRGs. The overlapping genes were defined as DEFRGs.

Gene ontology (GO) and Kyoto Encyclopedia of Genes and Genomes (KEGG) enrichment analyses. GO annotation and KEGG pathway enrichment analysis of DEFRGs was performed using the 'cluster profiler' R package (v4.8.3) (27) and visualized using Sangerbox 3.0 (http://sangerbox.com/home.html) (28). P.adjust <0.05 was used to indicate statistically significant enrichment by DEFRGs.

PPI network and identification of key modules and hub genes. In the present study, the PPI network for DEFRGs was constructed using the online tool provided by the Search Tool for the Retrieval of Interacting Genes/Proteins (STRING) database (v11.09) (https://string-db.org/) (29). To visualize the resulting PPI network, Cytoscape (v3.7.2; Cytoscape Consortium) software (30) was used. Furthermore, using cytoHubba and the Maximal Clique Centrality (MCC) algorithm, and the MCODE plugin (24) (Cytoscape Consortium) (degree cutoff=2; node score cutoff=0.2; K-core=2), the genes were screened and the top 10 hub genes and key functional modules were identified.

Receiver operating characteristic curve (ROC) analysis. To evaluate the diagnostic ability of the hub genes identified, ROC curves were constructed using data from the GSE26887 and GSE57338 databases. The area under the curve (AUC) was calculated and hub genes with AUC >0.7 were considered to have favorable diagnostic potential.

Cell culture and treatment. H9c2 cardiomyocytes were purchased from the Cell Bank/Stem Cell Bank (Chinese Academy of Sciences). All cells were cultured in DMEM (Hyclone; Cytiva) with 10% FBS (HyClone; Cytiva) and placed in a 37˚C incubator under standard conditions (5% CO_2, 95% humidity and 21% O_2 concentration) for 24 h.

H9c2 cells were separated into three groups: i) Control, ii) A/R and iii) A/R + ferrostatin-1 (Fer-1). The control group cells were incubated with normal medium (37˚C; 5% CO_2; 95% humidity and 21% O_2 concentration) for 24 h. As with previous studies (31,32), the A/R group was induced by 4 h anoxia and 4 h reoxygenation. The H9c2 cells were exposed to anoxic conditions by adding fresh anoxia medium (1 mM

$CaCl_2$, 10 mM KCl, 20 mM HEPES, 98.5 mM NaCl, 1.2 mM $MgSO_4$, 6 mM $NaHCO_3$, 0.9 mM NaH_2PO_4 and 40 mM sodium lactate; pH 6.8) and then incubated in a 37˚C chamber with an atmosphere of 95% N_2 and 5% CO_2 for 4 h. Following 4 h of anoxia, the anoxia medium was removed from the cells and a reoxygenation medium (1 mM $CaCl_2$, 5.5 mM glucose, 5 mM KCl, 20 mM HEPES, 129.5 mM NaCl, 1.2 mM $MgSO_4$, 20 mM $NaHCO_3$ and 0.9 mM NaH_2PO_4; pH 7.4) was added. The cells were then incubated in a 37˚C incubator with an atmosphere of 95% O_2 and 5% CO_2 for 4 h. Fer-1 (5 μM; MedChemExpress) pretreatment was added to the A/R + Fer-1 group in a 37˚C chamber under standard conditions (5% CO_2; 95% humidity and 21% O_2 concentration) for 2 h to inhibit ferroptosis.

Evaluation of cell viability. Cell viability was assessed using the Cell Counting Kit-8 (CCK-8) assay (cat. no. GK10001; GlpBio Technology, Inc.) based on the suggested procedure. Briefly, H9c2 cells were plated into a 96-well plate at a density of $5x10^3$ cells/well and CCK-8 solution was added to each well at a final concentration of 10% and incubated for 1 h at room temperature. The optical density (OD) value at 450 nm was measured using Spark® multimode microplate reader (Thermo Fisher Scientific, Inc.).

Western blot analysis. Proteins were extracted from the lysates of the H9c2 cells using RIPA lysis buffer (Beijing Solarbio Science & Technology Co., Ltd.), which contained 1% PMSF. The extracted proteins were determined using a BCA kit (GlpBio Technology, Inc.). Proteins were denatured through boiling for 5 min and then separated using 12% SDS-PAGE with a protein mass of 40 μg per lane. The separated proteins were then transferred onto PVDF membranes (MilliporeSigma). The membranes were then blocked with 5% non-fat dry milk for 2 h at room temperature, followed by incubation overnight at 4˚C with the following primary antibodies: Prostaglandin-endoperoxide synthase 2 (PTGS2; 1:500; cat. no. R23969; Chengdu Zen-Bioscience Co., Ltd), glutathione peroxidase 4 (GPX4; 1:1,000; cat. no. 381958; Chengdu Zen-Bioscience Co., Ltd.) and β-actin (1:1,000; cat. no. GB113225-100; Wuhan Servicebio Technology Co., Ltd.). Subsequently, the membranes were incubated with horseradish peroxidase-conjugated secondary antibodies (1:2,000; cat. no. A0239; Beyotime Institute of Biotechnology) for 2 h at room temperature. Positive blots were visualized using the Ultra High Sensitivity ECL kit (cat. no. GK10008; GlpBio Technology, Inc.) and imaged using the FluorChem FC3 System (ProteinSimple). Finally, the densitometric scanning of the blots were calculated using ImageJ software (v1.8.0.345; National Institutes of Health). β-actin was selected as the internal reference.

Measurement of intracellular reactive oxygen species (ROS). To determine the intracellular levels of ROS, the ROS Detection Kit (cat. no. S0033M; Beyotime Institute of Biotechnology) was used. H9c2 cells were seeded in a 6-well plate at a density of $1x10^5$ cells per well. After incubation and treatment as aforementioned, H9c2 cells were incubated with 2',7'-Dichlorodihydrofluorescein diacetate for 30 min at 37˚C in the dark according to the manufacturer's instructions. Subsequently, a fluorescence microscope (Olympus Corporation) was used to observe the associated alterations.

Iron content detection. Total iron content in H9c2 cells was obtained using a Total Iron Content Colorimetric Assay Kit (cat. no. E1042; Applygen Technologies, Inc.). H9c2 cells were lysed at 4˚C for 20 min, the cell lysate was centrifuged at 12,000 x g for 5 min at 4˚C and the total iron ion content was measured according to the manufacturer's instructions. The OD value was determined using the Spark multimode microplate reader (Thermo Fisher Scientific, Inc.).

Detection of antioxidant enzymes activities and lipid peroxidation. Treated H9c2 cells were lysed at 4˚C for 20 min and centrifuged at 12,000 x g for 10 or 5 min at 4˚C to remove cell debris. The malondialdehyde (MDA), superoxide dismutase (SOD), glutathione (GSH) and glutathione disulfide (GSSG) contents, and the GSH/GSSG ratio in H9c2 cells were measured according to the manufacturer's instructions of the Lipid Peroxidation MDA Assay Kit (cat. no. S01031S; Beyotime Institute of Biotechnology), Total Superoxide Dismutase Assay Kit with WST-8 (cat. no. S0101S; Beyotime Institute of Biotechnology), GSH and GSSG Assay Kit (cat. no. S0053; Beyotime Institute of Biotechnology), respectively. The OD value was determined using the Spark multimode microplate reader (Thermo Fisher Scientific, Inc.).

Reverse transcription (RT)-quantitative (q)PCR. H9c2 cells were subjected to RNA extraction using the TRIzol™ reagent (Invitrogen; Thermo Fisher Scientific, Inc.) to obtain total RNA. The quality and yield of the isolated RNA were assessed to confirm its suitability for evaluating mRNA expression. cDNA was produced by RT of total RNA using the HiScript® II 1st Strand cDNA Synthesis Kit (cat. no. R211-01; Vazyme Biotech Co., Ltd.). Briefly, 20 μl RT system (1 μg RNA, 10 μl RT mix, 2 μl HiScript II Enzyme Mix, 1 μl oligo, 1 μl random hexamers and RNase-free double-distilled H_2O) was converted to cDNA using the Bio-Rad PCR T100 Thermal Cycler (Bio-Rad Laboratories, Inc.) at 25˚C for 5 min, 50˚C for 15 min and 85˚C for 2 min. Subsequently, using the SYBR Green qPCR Master Mix (cat. no. B21203; Bimake.com), the level of gene expression was determined by qPCR and normalized to the level of β-actin. Briefly, 20 μl qPCR system (2 μl cDNA, 10 μl SYBR Green qPCR Master Mix, 1 μl forward primers, 1 μl reverse primers and 6 μl RNase-free double-distilled H_2O) was amplified by BIO-RAD CFX Connect Real-Time PCR Detection Systems (Bio-Rad Laboratories, Inc.). The procedure was as follows: Denaturation at 95˚C for 10 min, followed by thermal cycling at 95˚C for 15 sec and denaturation at 60˚C for 1 min, repeated for 40 cycles. Relative mRNA expression levels were calculated using the $2^{-\Delta\Delta Cq}$ method (33). The primers used in the present study were designed and synthesized by Sangon Biotech Co., Ltd. (Shanghai, China). Table SII provides details on the primers used.

Potential therapeutic drug prediction. Data on protein-drug interactions from the DSigDB (34) were used to predict the potential impact of drugs on ferroptosis in the context of ICM. The Drugbank database (35) was used to identify the chemical structures of the predicted drugs.

Statistical analysis. The results are presented as either the mean ± standard deviation or the mean ± standard error of

the mean. Statistical analyses were performed in GraphPad Prism 8 (v8.0.2; Dotmatics). To compare differences between two groups, the unpaired two-tailed Student's t-test was used. For comparisons between ≥3 groups, one-way analysis of variance and Dunnett's post hoc multiple comparison test was used. $P<0.05$ was used to indicate a statistically significant difference.

Results

Overall study protocol. The present study followed the flowchart presented in Fig. 1. Transcriptomic data obtained from the GSE26887 dataset available in the GEO public database, with data from 12 samples of post-ischemic myocardium and 5 samples of non-heart failure heart-matched donor heart.

Altered transcriptome in ICM is associated with the dysregulation of genes related to ferroptosis. GSEA is a widely-utilized method for evaluating the pertinence of defined gene sets with respect to the disease phenotype in disease transcriptomes (36). GSEA was used to assess the variation of FRGs in the transcriptome of individuals with ICM vs. the control group, as presented in Fig. 2. GSEA revealed significant dysregulation of FRGs between the two groups (NES=1.736; P.adjust <0.005; Fig. 2A). This suggests that FRGs are a crucial feature of ICM and their dysregulation provides evidence for the association between ICM and ferroptosis.

Identification of differentially expressed genes. Following the division of data from GSE26887 into normal and ICM groups, a differential analysis was performed using the 'limma' R package and 1,524 DEGs were identified with significance set at FDR <0.05 and $\log_2$FC >0.5 (Table SIII). Among these, 669 exhibited low expression and 855 showed high expression. These results are presented using a heat map (Fig. 2B) and a volcano plot (Fig. 2C), revealing distinct differential expression profiles of the DEGs between the ICM and control samples.

WGCNA. WGCNA is an analytical method used to analyze gene expression patterns of multiple samples, which can cluster genes with similar expression patterns. It has been widely used in several studies such as in gene association analysis (37).

Firstly, cluster analysis was performed using the 'flashClust' (v1.01-2-3) (22) function in WGCNA package with a threshold of 70, and cluster 1 was found to contain 17 samples. The sample clustering tree is shown in Fig. 3A, and the normal control and ICM groups were clustered separately. Secondly, a soft threshold of β=7 (scale-free R2=9; Fig. 3B) was used to establish a scale-free network. Thirdly, the threshold was set at 0.25 and the minimum number of modules was set at 50 to amalgamate comparable modules in a cluster. A total of six modules were created, each containing genes with comparable patterns of expression (Fig. 3C). The analysis of module-trait associations revealed that several modules were linked to ICM. The turquoise module, consisting of 683 genes, was found to have the strongest correlation with ICM (r=0.81; $P=8\times10^{-5}$; Fig. 3D and E). The correlation between the genes within the turquoise module and the ICM genes was significant (correlation=0.66; $P=4.8\times10^{-81}$; Fig. 3F).

Identification of DEFRGs. After the aforementioned screening process, 1,524 DEGs, 638 turquoise module genes identified by WGCNA, and 484 FRGs were overlapped, resulting in 19 genes (Table SIV) for further analysis (Fig. 4A). A clustered heatmap (Fig. 4B) and a correlation heatmap (Fig. 4C) were generated to display the differences in expression and correlation of the 19 DEFRGs between ischemic cardiac tissue and normal control cardiac tissue.

GO and KEGG analyses. To understand the functions and pathways associated with DEFRGs, enrichment analyses were performed for GO and KEGG pathways. The DEFRGs were primarily associated with the biological processes of cellular iron ion homeostasis and negative regulation of transferase activity, positive regulation of peptidyl serine phosphorylation, smooth muscle cell proliferation, and tissue remodeling (Fig. 5A). Among the molecular functions, the DEFRGs were also involved in other processes such as heat shock protein and iron ion binding, protein kinase inhibitor activity, virus receptor activity and exogenous protein binding (Fig. 5B). The DEFRGs were found to be localized in several cellular components, such as the basal plasma membrane, cellular basal fraction and secretory granule membrane (Fig. 5C). KEGG enrichment analysis revealed that the DEFRGs were mainly associated with ferroptosis, hypoxia-inducible factor (HIF)-1 signaling and hematopoietic cell lineage pathways (Fig. 5D). Associations between genes and different functions or pathways were identified in gene and pathway cross-talk mapping and these findings indicate that multiple genes and pathways may be dysregulated in ICM (Fig. 5E-H).

Construction of PPI network and identification of key module and hub genes. As the regulatory role of FRGs in ICM involves the cross-talk of multiple gene functions and pathways, a PPI network of DEFRGs was constructed (Fig. 6A) using the STRING database and functional modules and key genes in the PPI network were searched for using Cytoscape software. Using cytoHubba and the MCC algorithm, and the MCODE plugin for gene screening, the key functional and top 10 hub genes were identified: Interleukin-6 (IL6), Transferrin receptor protein 1 (TFRC), Gap junction α-1 protein (GJA1), CD44 antigen (CD44), Cytochrome b-245 heavy chain (CYBB), Metalloproteinase inhibitor 1 (TIMP1), α-synuclein (SNCA), Cyclin-dependent kinase inhibitor 1 (CDKN1A), Solute carrier family 40 member 1 (SLC40A1), Stearoyl-CoA desaturase (SCD) (Fig. 6C), and key modules (Fig. 6B). Notably, the key modules completely overlapped with the hub genes. Fig. 6D shows the differential expression of hub genes in ICM. Moreover, it was found that the hub genes were associated with other DEFRGs in ICM (Fig. 6E), which indicated that the hub genes may regulate ferroptosis through multiple genes in ICM.

Exploration of the diagnostic capability of hub genes. The diagnostic capability of hub genes in the GSE26887 and GSE57338 datasets were assessed. In the GSE26887 dataset, the expression of hub genes was compared, and the screened hub genes were demonstrated to be significantly different in both ICM and normal heart tissues (Fig. 7A). ROC analysis

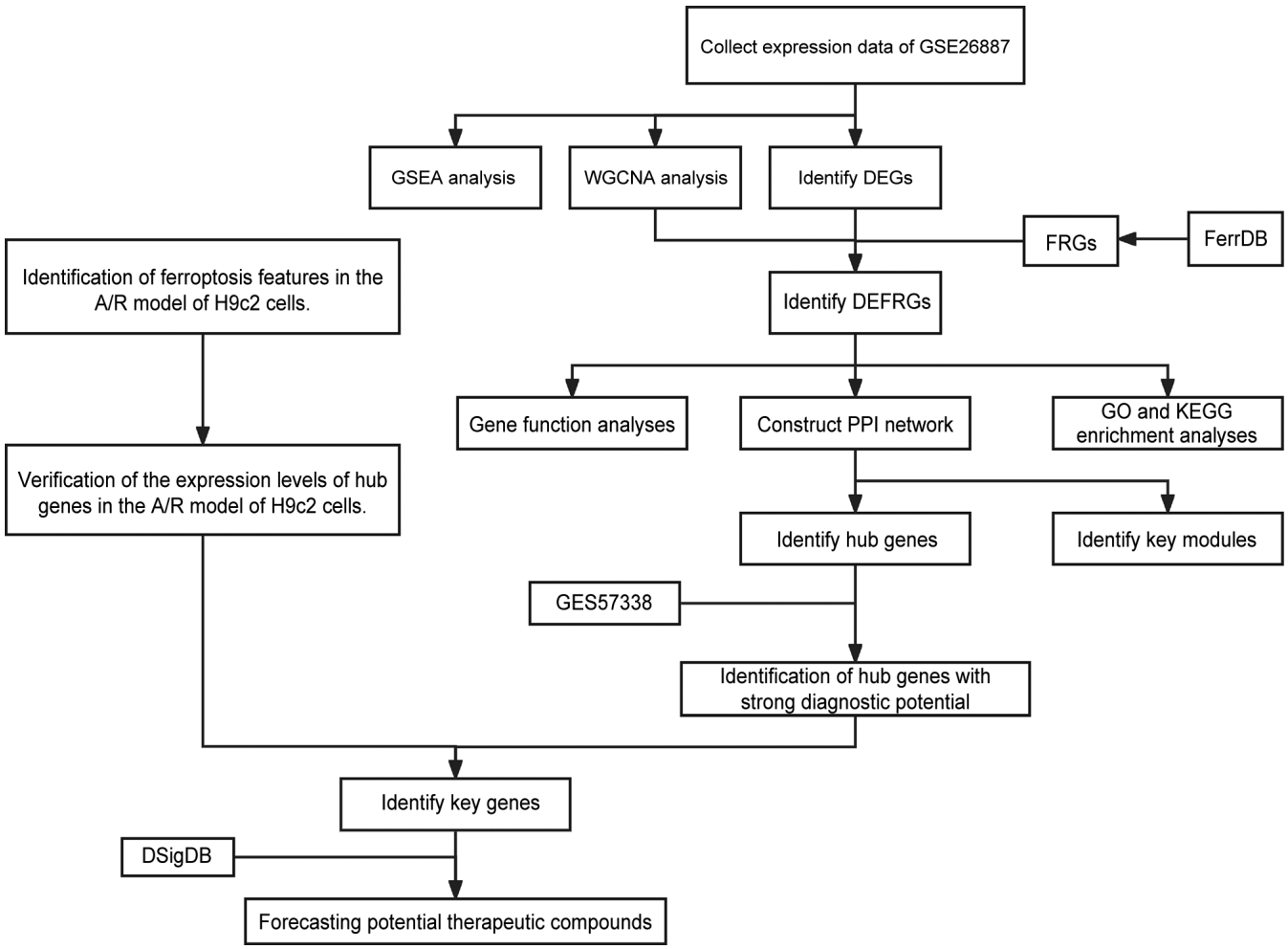

Figure 1. Overall protocol of the present study. GSEA, gene set enrichment analysis; WGCNA, weighted gene co-expression network analysis; DEG, differentially expressed genes; A/R, anoxic reoxygenation; FRG, ferroptosis-related gene; DEFRG, differentially expressed FRG; PPI, protein-protein interaction; GO, Gene Ontology; KEGG, Kyoto Encyclopedia of Genes and Genomes; DSigDB, Drug Signatures Database.

results confirmed the association between the hub genes and ICM. Additionally, the diagnostic potential of these genes was favorable (AUC >0.7; Fig. 7B) (38). Subsequently, validation of the hub genes was performed based on the GSE57338 dataset. Fig. 7C demonstrates that *IL-6* and *CD44* were not elevated in the samples with ICM and did not significantly differ from normal samples; however, *GJA1*, *SNCA*, and *SLC40A1* had significantly higher gene expression in ICM samples, and *TFRC*, *TIMP1*, *CDKN1A*, *SCD* and *CYBB* had significantly lower gene expression in ICM samples compared with the normal samples. The diagnostic ability of the hub genes was then further validated, in which *TFRC*, *IL-6* and *CD44* were unable to effectively diagnose ICM and the diagnostic potential of *SCD* was weak; however, the other hub genes demonstrated good diagnostic ability (Fig. 7D). The aforementioned genes were validated by multiple steps, and most of the FRGs demonstrated good diagnostic ability, suggesting that there may be a connection between ferroptosis and ICM. Nevertheless, the significance of hub genes needs to be continued to be explored in subsequent studies.

Validation of hub gene expression in the H9c2 A/R injury model. To confirm whether the ferroptosis inhibitor Fer-1 pretreatment can attenuate ferroptosis and protect cardiomyocytes from the impact of A/R injury, a A/R cellular injury model was established using H9c2 cells. The H9c2 cells were subjected to A/R treatment to simulate myocardial I/R injury, and the extent of ferroptosis in the model, as well as the changes in FRGs, were detected. Firstly, the changes in GPX4 and PTGS2 were assessed at the protein level, which are widely used as indicators for detecting the occurrence of ferroptosis (10). The protein level of GPX4 in A/R treated H9c2 cells significantly decreased in comparison with control, whilst the protein level of PTGS2 in A/R treated H9c2 cells significantly increased in comparison with control correspondingly; however, these changes were reversed by pretreatment with Fer-1 (Fig. 8A and B). Consistently, H9c2 cells subjected to A/R treatment exhibited notably higher levels of intracellular ROS in comparison with control; however, intervention with Fer-1 resulted in a marked decrease in ROS levels in comparison with A/R (Fig. 8C). In subsequent experiments, the cell viability assay revealed that A/R treated H9c2 cells had lower cell viability compared with the control; however, Fer-1 intervention increased the cell viability of H9c2 cells compared with A/R (Fig. 8D). In addition, significantly increased levels of total iron (Fig. 8E),

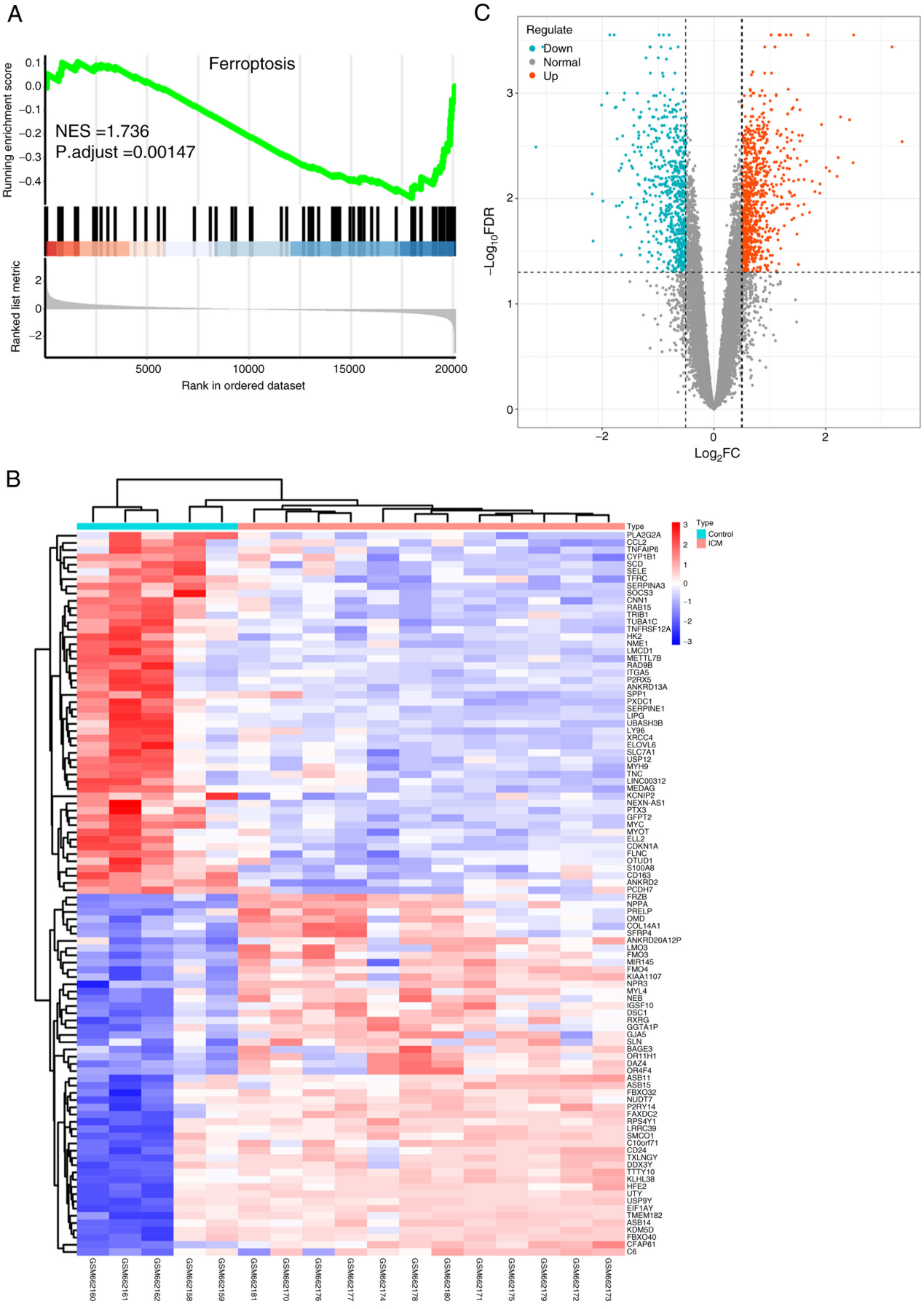

Figure 2. GSEA and identification of differentially expressed genes. (A) GSEA of ferroptosis-related genes in GSE26887. (B) Heatmap clustering of genes with markedly different expression in ICM compared with normal control samples. $\log_2$FC >0.5 and adjusted P<0.05 were used to define statistically significant DEGs. (C) Volcano plot of DEGs in GSE26887. The blue dots represent low expression and the red dots represent high expression. GSEA, gene set enrichment analysis; DEG, differentially expressed gene; NES, normalized enrichment score; FDR, false discovery rate; FC, fold change; ICM, ischemic cardiomyopathy.

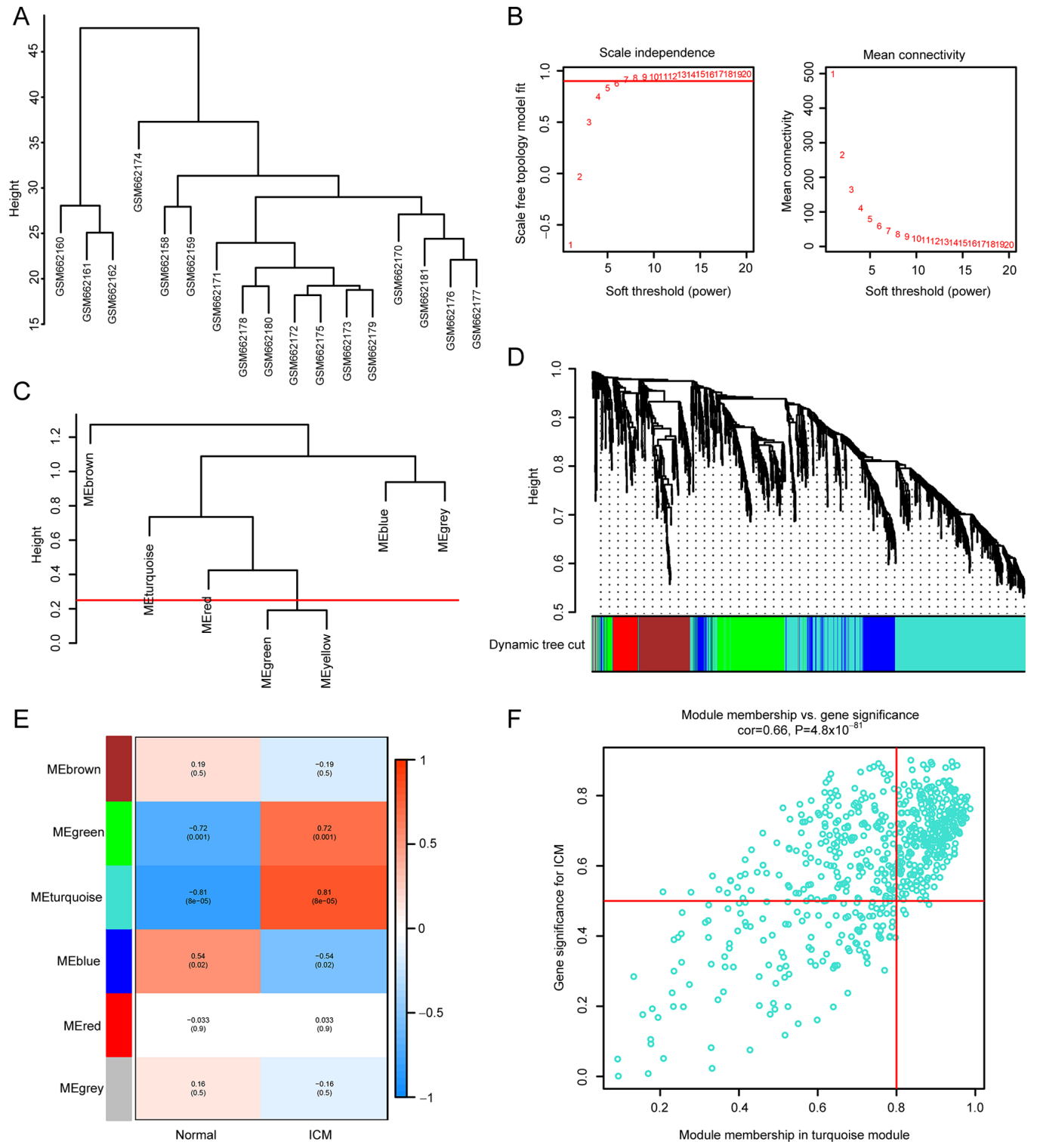

Figure 3. Construction and module analysis of weighted gene co-expression network analysis. (A) Sample clustering dendrogram based on Euclidean distance to detect outliers. (B) Network topology analysis under several soft-threshold powers. (C) Clustering of module eigengenes with the threshold set at 0.25 to merge the modules that were comparable in the cluster tree. (D) Clustering dendrogram of genes with different similarities based on topological overlap and the assigned module color (Gene Expression Omnibus). (E) Module-trait relationships (Gene Expression Omnibus). Different modules were produced, shown in different colors by aggregating genes with strong correlations into the same module. The turquoise module has a stronger correlation with ICM than the other modules. (F) Relevance of members in the turquoise module and ICM. ICM, ischemic cardiomyopathy; cor, correlation.

MDA (Fig. 8F) and GSSG (Fig. 8G), significantly decreased levels of GSH (Fig. 8H), GSH/GSSG ratio (Fig. 8I) and SOD (Fig. 8J) were observed in A/R treated H9c2 cells compared with the control. These findings indicate the presence of ferroptosis during the process of A/R.

Disruption of FRGs was also observed in the transcriptomics of human ischemic myocardium samples. The transcription levels of hub genes in the A/R model were assessed and the qPCR results showed that 3/7 hub genes (*GJA1*, *SCL40A1* and *SNCA*; Fig. 8K-Q) were significantly

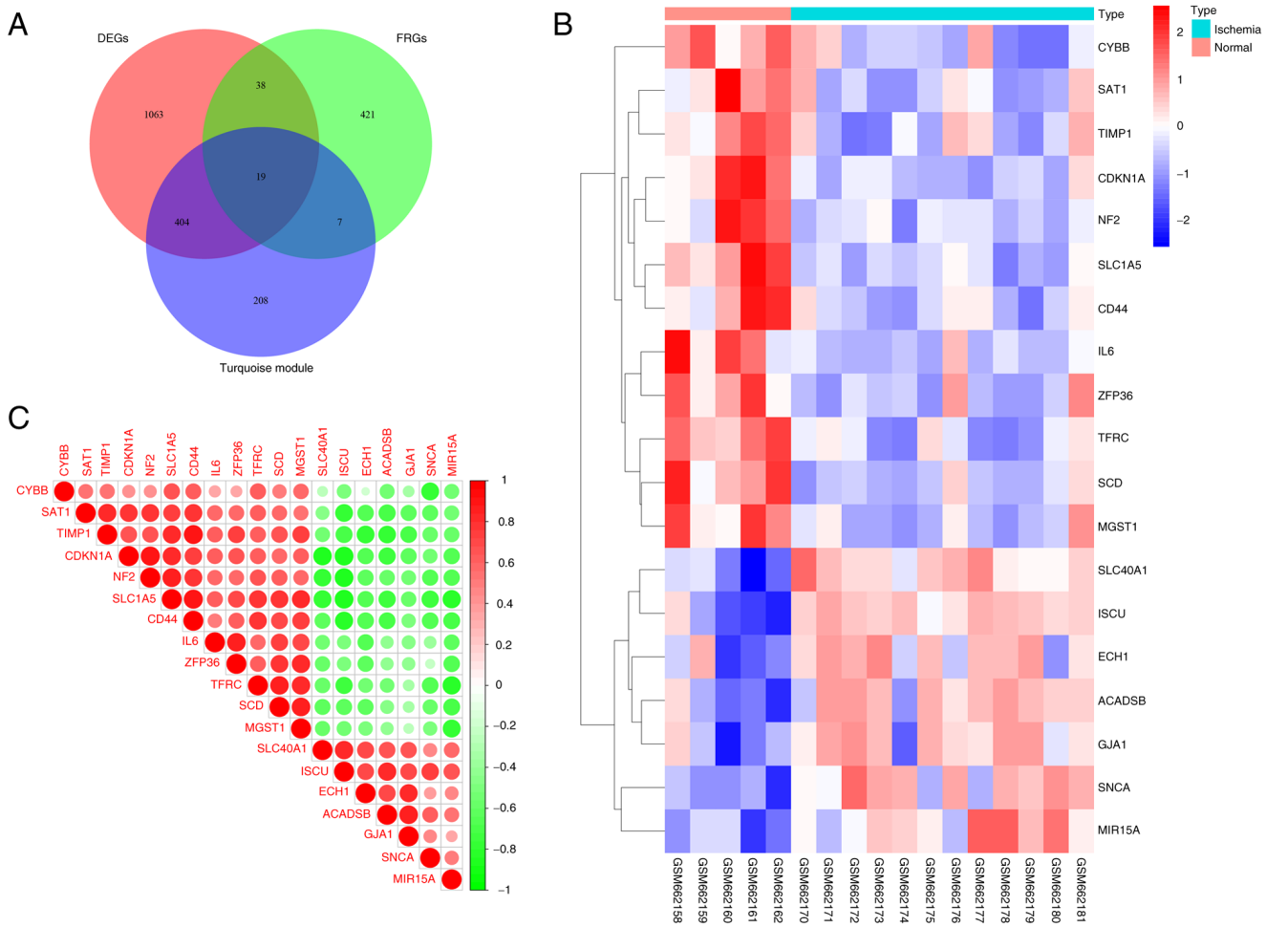

Figure 4. Identification of DEFRGs. (A) Venn diagram showing the overlay of the turquoise modules, DEGs and FRGs. (B) Clustered heatmap of DEFRGs in the GSE26887 dataset. (C) Correlation heatmap of DEFRGs in ischemic cardiomyopathy from the GSE26887 dataset. DEG, differentially expressed gene; FRG, ferroptosis-related gene; DEFRG, differentially expressed ferroptosis-related gene.

differentially elevated in the model group compared with the control and were significantly alleviated by the addition of Fer-1 intervention, indicating that they were involved in the regulation of ICM ferroptosis. Thus, it was demonstrated that *GJA1*, *SCL40A1* and *SNCA* are key genes regulating ferroptosis in ICM.

Potential ferroptosis-regulating drugs prediction. The DSigDB was used to predict potential ferroptosis-regulating drugs associated with key genes that may treat ICM by modulating ferroptosis. A final total of 233 drugs was obtained and their combination scores and corresponding target genes are listed in Table SV. The drugs with the highest combined scores were retinoic acid and benzo[a]pyrene (Fig. 9A). Retinoic acid (combined scores=219193; Fig. 9B) had a strong drug-target association (P.adjust <0.05; Fig. 9C). By contrast, benzo[a]pyrene is strongly toxicogenic and may accelerate the process of ferroptosis, requiring protection in daily life species (39).

Discussion

Globally, ICM is a principal contributor to mortality, sickness and incapacity arising from cardiovascular disease (40,41). Therefore, it is urgent to identify the pathophysiological mechanisms of ICM and provide meaningful diagnostic and therapeutic targets for clinical work (7).

Ferroptosis is an iron-dependent and distinct form of regulated cell death, differing from apoptosis, necrosis and autophagy (9). It is characterized by the accumulation of lipid hydroperoxides that reach lethal levels, causing oxidative damage to the cellular membrane (9,10). In the past decade, an increasing number of studies have supported the important pathophysiological role of ferroptosis in the development of cardiovascular diseases such as doxorubicin-induced cardiomyopathy, myocardial I/R injury, myocardial infarction and heart failure (42). High levels of ferroptosis, mediated by certain signaling and metabolic pathways, may result in more severe injury to ICM, and the regulatory molecular mechanisms and signaling pathway cross-talk remain unclear (43). The rapid advancement of transcriptomics has offered new insights into the pathological process of ferroptosis in ICM (44). The present study comprehensively analyzed the dysregulated ferroptosis-related genes in the transcriptome of ICM, explored related functions and pathways through GO and KEGG enrichment analysis, predicted hub genes through the PPI network, analyzed their diagnostic ability through

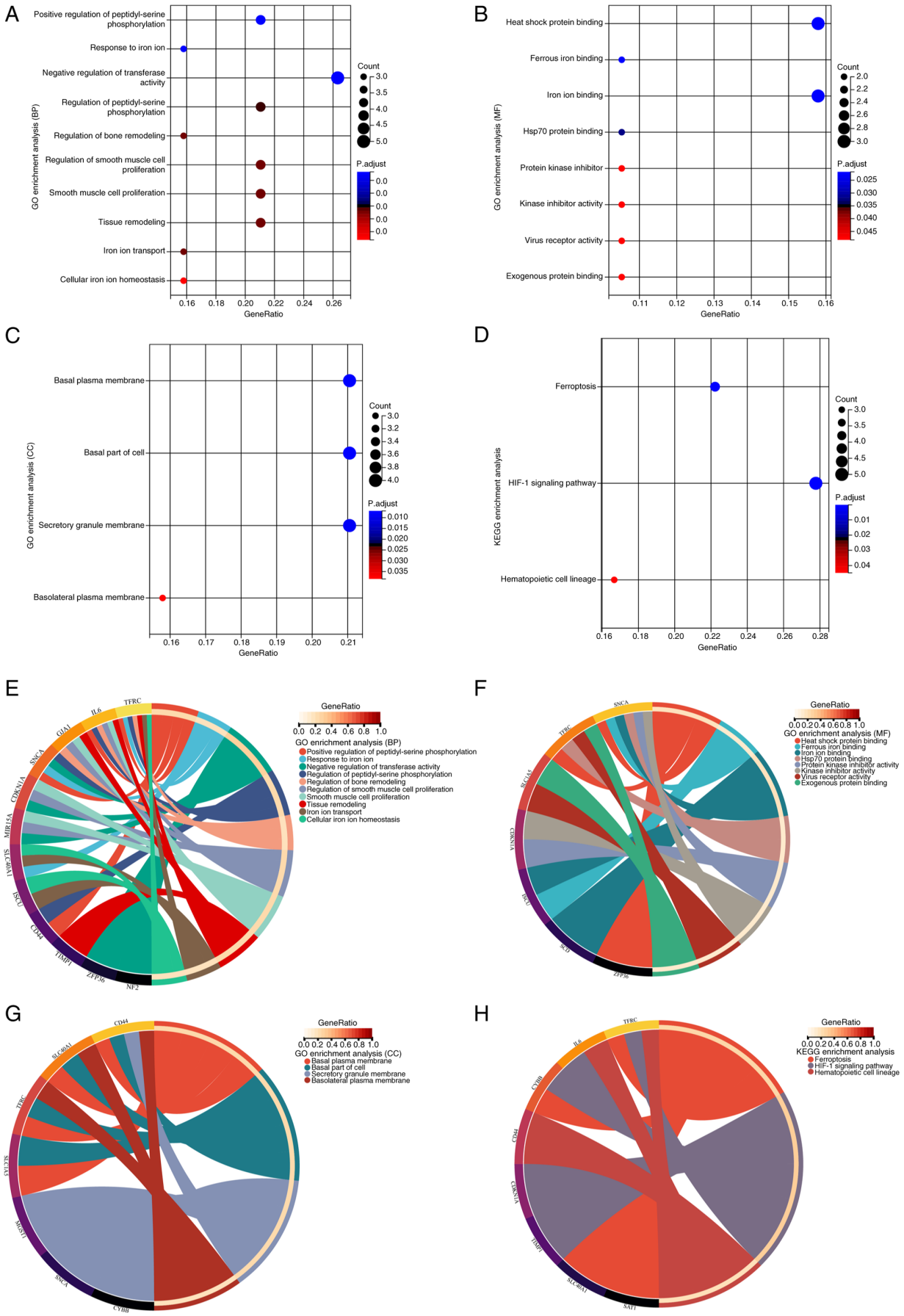

Figure 5. GO and KEGG enrichment analyses of DEFRGs. GO enrichment analysis of DEFRGs in the (A) BP, (B) MF and (C) CC categories. (D) KEGG enrichment analysis of DEFRGs. Crosstalk analysis between DEFRGs and gene functions in (E) BP, (F) MF, (G) CC and (H) KEGG pathways. GO, Gene Ontology; KEGG, Kyoto Encyclopedia of Genes and Genomes; DEFRG, differentially expressed ferroptosis-related genes; BP, biological process; MF, molecular function; CC, cellular component.

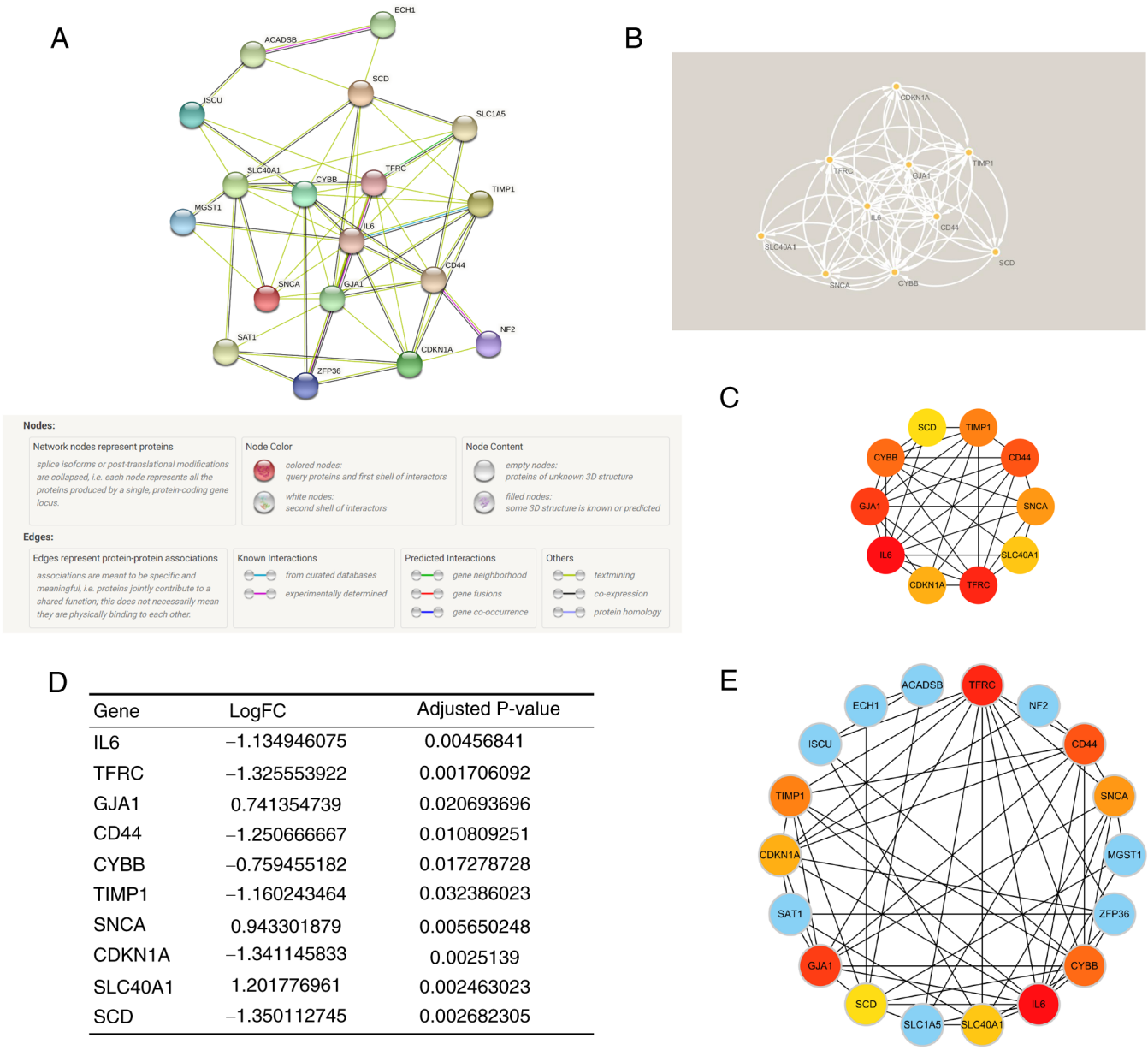

Gene	LogFC	Adjusted P-value
IL6	−1.134946075	0.00456841
TFRC	−1.325553922	0.001706092
GJA1	0.741354739	0.020693696
CD44	−1.250666667	0.010809251
CYBB	−0.759455182	0.017278728
TIMP1	−1.160243464	0.032386023
SNCA	0.943301879	0.005650248
CDKN1A	−1.341145833	0.0025139
SLC40A1	1.201776961	0.002463023
SCD	−1.350112745	0.002682305

Figure 6. PPI network and identification of hub genes and module. (A) A total of 18 DEFRGs in the PPI network, constructed using the Search Tool for the Retrieval of Interacting Genes/Proteins database, in which MIR15A was not associated with other DEFRGs (minimum required interaction score=0.4). (B) Modules identified using the MCODE plugin and the K-means clustering algorithm (degree cutoff=2; node score cutoff=0.2; K-core=2). (C) Crosstalk between 10 hub genes, in which the deepness of the dot color indicates that the rank order of the hub gene is higher. (D) Differential expression of hub genes in ischemic cardiomyopathy. (E) Crosstalk between the top 10 hub genes ranked by the Maximal Clique Centrality algorithm and other DEFRGs. PPI, protein-protein interaction; DEFRG, differentially expressed ferroptosis-related gene; FC, fold change.

ROC curves, and assessed hub genes in *in vitro* models. Finally, potential ferroptosis-targeted drugs were obtained from the DSigDB, providing several potential choices for the clinical treatment of ICM.

In the present study, GSEA demonstrated a correlation between ferroptosis and ICM, which is consistent with previous research results, indicating the presence of ferroptosis in the pathological process of ICM (44-46). WGCNA and differential analysis identified clustered modules and dysregulated FRGs in ICM, and subsequent GO enrichment analysis revealed that the dysregulated FRGs in the ICM are involved in the regulation of ferroptosis through several pathways.

Iron is a crucial micronutrient within the human body as it serves a vital role in biological processes, including the transportation, storage and utilization of oxygen (47). Iron homeostasis serves a crucial role in the function of the heart. Most iron ions are transported through transport proteins on the basal membrane, and intracellular iron ions can also bind to ferritin and are secreted through the multivesicular body-exosome pathway (48). FRGs negatively regulate cellular iron homeostasis and transferase activity, causing iron ions to accumulate in the mitochondria, increasing oxidative stress and ultimately leading to mitochondrial dysfunction (49). Due to the limited regenerative capacity of cardiomyocytes, a stable scar is formed

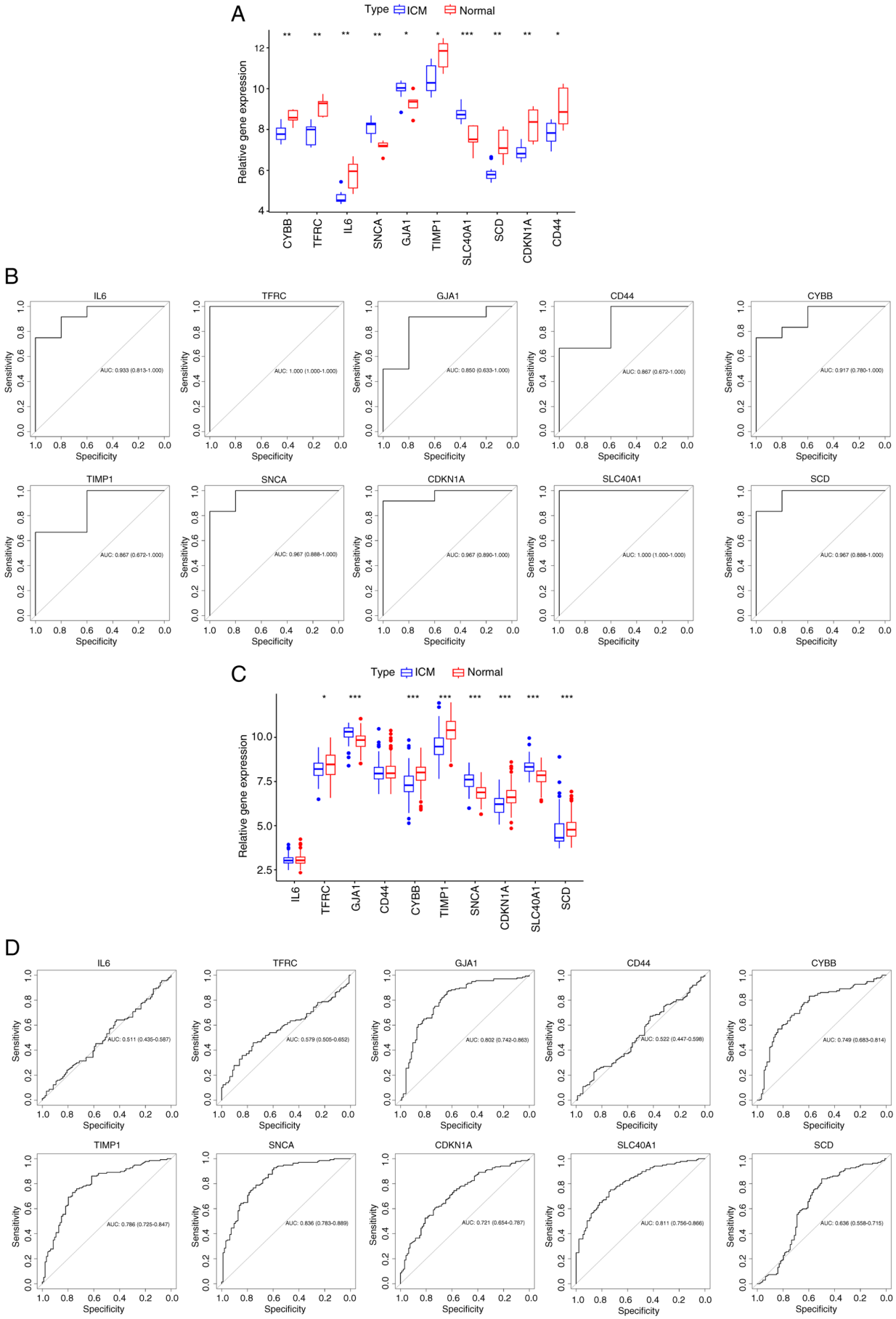

Figure 7. Exploration of the diagnostic capability of key genes. (A) Relative expression of hub genes in GSE26887. (B) ROC curves show the diagnostic capability of hub genes for ICM in GSE26887. (C) Relative expression of hub genes in GSE57338. (D) ROC curves show the diagnostic capability of hub genes for ICM in GSE57338. n≥3. *P<0.05; **P<0.01; ***P<0.001. ROC, receiver operating characteristic; ICM, ischemic cardiomyopathy; AUC, areas under the curve.

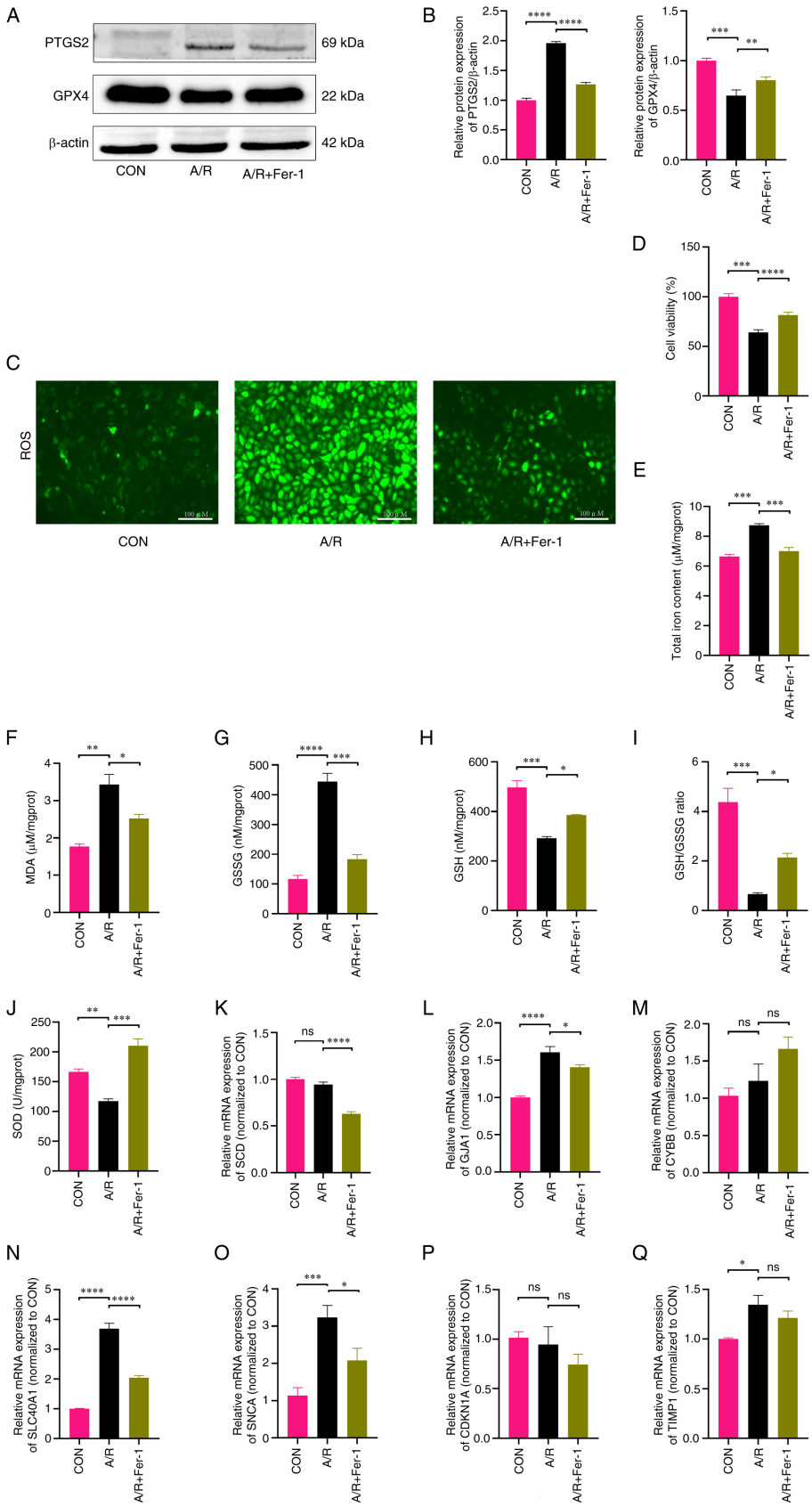

Figure 8. Altered ferroptosis level and assessment of hub gene expression in the H9c2 A/R injury model. (A) Representative western blotting bands of PTGS2 and GPX4. (B) Relative protein expression levels of PTGS2 and GPX4, estimated using ImageJ software. (C) Representative images of ROS content in H9c2 myofibroblasts. (D) Cell viability was assessed using the Cell Counting Kit-8 assay. H9c2 cell levels of (E) total iron, (F) MDA, (G) GSSG, (H) GSH, (I) GSH/GSSG ratios and (J) SOD in each group. Reverse transcription-quantitative PCR results of (K) SCD, (L) GJA1, (M) CYBB, (N) SLC40A1, (O) SNCA, (P) CDKN1A and (Q) TIMP1. n≥3. *P<0.05; **P<0.01; ***P<0.001; ****P<0.0001. A/R, anoxic reoxygenation; PTGS2, prostaglandin-endoperoxide synthase 2; GPX4, glutathione peroxidase 4; ROS, reactive oxygen species; SOD, superoxide dismutase; GSH, glutathione; GSSG, glutathione disulfide; MDA, malondialdehyde; ns, not significant; CON, control; Fer-1, ferrostatin-1; SCD, Stearoyl-CoA desaturase; GJA1, Gap junction alpha-1 protein; CYBB, Cytochrome b-245 heavy chain; SLC40A1, Solute carrier family 40 member 1; SNCA, Alpha-synuclein; CDKN1A, Cyclin-dependent kinase inhibitor 1; TIMP1, Metalloproteinase inhibitor 1.

A

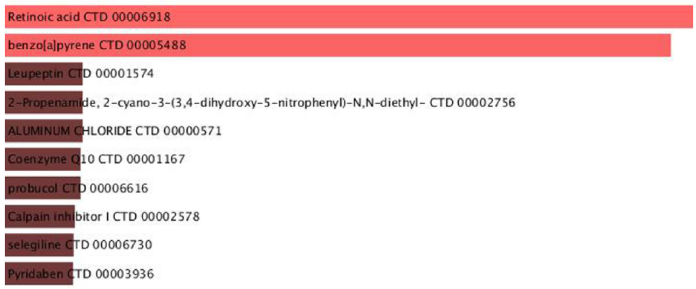

B

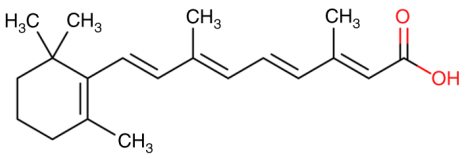

C

Predicted drug	Target genes	Odds ratio	Combined score	P-value	Adjusted P-value
Retinoic acid CTD 00006918	GJA1;SLC40A1;SNCA	47226	219193.0129	0.009644542	0.031893861
Benzo[a]pyrene CTD 00005488	GJA1;SLC40A1;SNCA	46728	211519.0601	0.010817371	0.03301494

Figure 9. Targeted drugs prediction. (A) Top 10 predicted targeted drugs ranked according to combined score in the Drug Signatures Database. (B) Chemical structure of retinoic acid. (C) Details of the drugs with strong drug-target associations.

immediately after myocardial ischemia. However, under the stimulation of chronic ischemia, the excessive deposition of collagen-rich extracellular matrix determines the pathological remodeling of the myocardium and causes an increase in mechanical strain in the border zone, which may lead to expansion of the fibrotic area, decreased tissue compliance and increased cardiac afterload (50-54). Existing research indicates that regulating FRGs can effectively reduce cardiac injury, fibrosis and pathological remodeling during ischemia (55). In the present study, the DEFRGs were found to be enriched in iron metabolism and the HIF-1 signaling pathway. Additionally, they were linked to certain pathways of hematopoietic cell lines, which could be associated with the transportation of iron ions. These findings indicate that the regulation of ferroptosis in ICM involves unknown key molecules and pathways that require further exploration. To gain a more thorough understanding of the mechanism behind iron metabolism in ICM, additional research is necessary.

By constructing the PPI interaction network to identify the top 10 hub genes based on the MCC algorithm. The diagnostic ability of hub genes was determined by ROC, and genes with weak diagnostic ability were excluded. In order to more realistically verify the expression of the remaining hub genes, the H9c2 A/R injury model was further constructed to verify whether the expression trend of the remaining hub genes was consistent with the transcriptomics data. In the present study, *GJA1*, *SCL40A1* and *SNCA* showed promise as therapeutic targets for ICM. The upregulation of *SNCA* leads to cells being subjected to abnormal ROS generation and glutathione utilization, resulting in oxidative stress of lipid peroxidation and eventual cell death via ferroptosis (56). Notably, upon activation of ferroptosis, *GJA1* is markedly upregulated as a negative regulatory gene. However, the mechanism of *GJA1* in the ferroptosis pathway remains incompletely understood, potentially as a result of its bidirectional regulatory effect on ferroptosis which has yet to be acknowledged (57,58). Further research is necessary to supplement this. Furthermore, as a positive regulatory gene, *SCL40A1* notably increased in an A/R model, resulting in cell iron overload and ferroptosis (59). The aforementioned hub genes are expected to become new targets for the treatment of ICM, and further investigation into their specific regulatory mechanisms is required.

The present study aimed to regulate dysregulated genes in ICM for treatment and clinical transformation. According to the selected hub genes in the present study, potential therapeutic drugs were predicted for ICM. Among them, retinoic acid and benzo[a]pyrene demonstrated a high drug target association. Retinoic acid is essential for maintaining tissue homeostasis and has been shown to ameliorate I/R injury and several instances of drug-induced cardiotoxicity (60). These effects are achieved through the inhibition of oxidative stress, prevention of cardiomyocyte apoptosis and attenuation of p38 MAPK, JNK and NF-κB activation (61-63). Benzo[a]pyrene is a polycyclic aromatic hydrocarbon present in tobacco smoke and indoor air pollution. It possesses attributes such as lipophilicity, refractoriness, bioaccumulation, cytotoxicity, mutagenicity and carcinogenicity (64,65). It may have a negative regulatory effect on I/R injury and lacks protective properties (39). As a result, it should be avoided in everyday circumstances. Similar protective medicines, such as retinoic acid, may regulate ferroptosis to reduce damage to the ICM. However, their pharmacological mechanisms have not yet been explored (66).

The analyses in the present study confirmed the presence of numerous dysregulated FGRs in ICM, providing evidence for subsequent exploration; however, it is worth noting that the present study has certain limitations. First, the present study observed that ferroptosis features in the H9c2 cell injury model, including intracellular ROS aggregation, ferroptosis marker protein changes and lipid peroxidation (44-46). Nevertheless, it did not investigate how dysregulation of DEFRGs regulates ferroptosis in ICM, which is a limitation of the present study. In addition, the present study did not directly observe the characteristics of ferroptosis in human ICM. To establish more dependable diagnostic and therapeutic targets,

and to translate the findings of the present study into clinical outcomes, in-depth mechanism and functional studies are imperative for comprehending the regulation of ferroptosis in ICM by the FGRs.

Overall, extensive dysregulation of ferroptosis-related genes was identified in ICM. These are situated in the basement membrane and secretory granules. They trigger intracellular iron overload through the transport function of iron ions, which may lead to positive regulatory peptide serine phosphorylation, smooth muscle cell proliferation and tissue remodeling. Furthermore, the expression of hub FRGs (*GJA1*, *SCL40A1*, *SNCA*) were assessed in an A/R model and a statistically significant association between *GJA1*, *SCL40A1*, *SNCA* and the occurrence of ICM was identified. In addition, the present research predicted that retinoic acid may provide a protective mechanism by regulating ferroptosis in ICM. The current study offers new insights and evidence regarding the involvement of ferroptosis in ICM. This is important for discovering the pathological mechanisms of ICM and identifying its diagnostic and therapeutic targets.

Acknowledgements

Not applicable.

Funding

The present study was supported by the National Nature Science Foundation of China (grant nos. 81860082 and 82160073) and Jiangxi Provincial Natural Science Foundation (grant nos. 20212ACB206011, 20224ACB206002 and 20232BAB206009).

Availability of data and materials

The data generated in the present study may be requested from the corresponding author.

Authors' contributions

STZ, ZCQ, RYZ performed the cellular experiments and participated in writing and data analysis. HXZ provided the experimental design. ZCQ and RYZ confirm the authenticity of all the raw data. RBQ and HZP analyzed the experimental data. LFZ and ZQX provided software support. SQL and LW designed the experiments and provided financial assistance. All authors have read and approved the final manuscript.

Ethics approval and consent to participate

Not applicable.

Patient consent for publication

Not applicable.

Competing interests

The authors declare that they have no competing interests.

References

1. Moroni F, Gertz Z and Azzalini L: Relief of ischemia in ischemic cardiomyopathy. Curr Cardiol Rep 23: 80, 2021.
2. Cabac-Pogorevici I, Muk B, Rustamova Y, Kalogeropoulos A, Tzeis S and Vardas P: Ischaemic cardiomyopathy. Pathophysiological insights, diagnostic management and the roles of revascularisation and device treatment. Gaps and dilemmas in the era of advanced technology. Eur J Heart Fail 22: 789-799, 2020.
3. Li Y, Du Y, Cao J, Gao Q, Li H, Chen Y and Lu N: MiR-130a inhibition protects rat cardiac myocytes from hypoxia-triggered apoptosis by targeting Smad4. Kardiol Pol 76: 993-1001, 2018.
4. Xu Q, Liu S, Gong Q, Zhu R, Liu J, Wu Q and Zhou X: Notch1 protects against ischemic-reperfusion injury by suppressing PTEN-Pink1-Mediated mitochondrial dysfunction and mitophagy. Cells 12: 137, 2022.
5. Wang X, Xie W, Zhang Y, Lin P, Han L, Han P, Wang Y, Chen Z, Ji G, Zheng M, *et al*: Cardioprotection of ischemia/reperfusion injury by cholesterol-dependent MG53-mediated membrane repair. Circ Res 107: 76-83, 2010.
6. Gao C, Wang R, Li B, Guo Y, Yin T, Xia Y, Zhang F, Lian K, Liu Y, Wang H, *et al*: TXNIP/Redd1 signalling and excessive autophagy: A novel mechanism of myocardial ischaemia/reperfusion injury in mice. Cardiovasc Res 116: 645-657, 2020.
7. Hausenloy DJ and Yellon DM: Myocardial ischemia-reperfusion injury: A neglected therapeutic target. J Clin Invest 123: 92-100, 2013.
8. Hao L, Wang J and Liu N: Long noncoding RNA TALNEC2 regulates myocardial ischemic injury in H9c2 cells by regulating miR-21/PDCD4-medited activation of Wnt/β-catenin pathway. J Cell Biochem 120: 12912-12923, 2019.
9. Dixon SJ, Lemberg KM, Lamprecht MR, Skouta R, Zaitsev EM, Gleason CE, Patel DN, Bauer AJ, Cantley AM, Yang WS, *et al*: Ferroptosis: An iron-dependent form of nonapoptotic cell death. Cell 149: 1060-1072, 2012.
10. Stockwell BR, Friedmann Angeli JP, Bayir H, Bush AI, Conrad M, Dixon SJ, Fulda S, Gascón S, Hatzios SK, Kagan VE, *et al*: Ferroptosis: A regulated cell death nexus linking metabolism, redox biology, and disease. Cell 171: 273-285, 2017.
11. Wang M, Mao C, Ouyang L, Liu Y, Lai W, Liu N, Shi Y, Chen L, Xiao D, Yu F, *et al*: Long noncoding RNA LINC00336 inhibits ferroptosis in lung cancer by functioning as a competing endogenous RNA. Cell Death Differ 26: 2329-2343, 2019.
12. Kenny EM, Fidan E, Yang Q, Anthonymuthu TS, New LA, Meyer EA, Wang H, Kochanek PM, Dixon CE, Kagan VE and Bayir H: Ferroptosis contributes to neuronal death and functional outcome after traumatic brain injury. Crit Care Med 47: 410-418, 2019.
13. Chen B, Chen Z, Liu M, Gao X, Cheng Y, Wei Y, Wu Z, Cui D and Shang H: Inhibition of neuronal ferroptosis in the acute phase of intracerebral hemorrhage shows long-term cerebroprotective effects. Brain Res Bull 153: 122-132, 2019.
14. Guan X, Li X, Yang X, Yan J, Shi P, Ba L, Cao Y and Wang P: The neuroprotective effects of carvacrol on ischemia/reperfusion-induced hippocampal neuronal impairment by ferroptosis mitigation. Life Sci 235: 116795, 2019.
15. Kobayashi M, Suhara T, Baba Y, Kawasaki NK, Higa JK and Matsui T: Pathological roles of iron in cardiovascular disease. Curr Drug Targets 19: 1068-1076, 2018.
16. Bulluck H, Rosmini S, Abdel-Gadir A, White SK, Bhuva AN, Treibel TA, Fontana M, Ramlall M, Hamarneh A, Sirker A, *et al*: Residual myocardial iron following intramyocardial hemorrhage during the convalescent phase of reperfused ST-Segment-Elevation myocardial infarction and adverse left ventricular remodeling. Circ Cardiovasc Imaging 9: e004940, 2016.
17. Li D, Pi W, Sun Z, Liu X and Jiang J: Ferroptosis and its role in cardiomyopathy. Biomed Pharmacother 153: 113279, 2022.
18. Greco S, Fasanaro P, Castelvecchio S, D'Alessandra Y, Arcelli D, Di Donato M, Malavazos A, Capogrossi MC, Menicanti L and Martelli F: MicroRNA dysregulation in diabetic ischemic heart failure patients. Diabetes 61: 1633-1641, 2012.
19. Liu Y, Morley M, Brandimarto J, Hannenhalli S, Hu Y, Ashley EA, Tang WH, Moravec CS, Margulies KB, Cappola TP, *et al*: RNA-Seq identifies novel myocardial gene expression signatures of heart failure. Genomics 105: 83-89, 2015.

20. Edgar R, Domrachev M and Lash AE: Gene expression omnibus: NCBI gene expression and hybridization array data repository. Nucleic Acids Res 30: 207-210, 2002.
21. Subramanian A, Tamayo P, Mootha VK, Mukherjee S, Ebert BL, Gillette MA, Paulovich A, Pomeroy SL, Golub TR, Lander ES and Mesirov JP: Gene set enrichment analysis: A knowledge-based approach for interpreting genome-wide expression profiles. Proc Natl Acad Sci USA 102: 15545-15550, 2005.
22. Langfelder P and Horvath S: WGCNA: An R package for weighted correlation network analysis. BMC Bioinformatics 9: 559, 2008.
23. Ritchie ME, Phipson B, Wu D, Hu Y, Law CW, Shi W and Smyth GK: limma powers differential expression analyses for RNA-sequencing and microarray studies. Nucleic Acids Res 43: e47, 2015.
24. Chin CH, Chen SH, Wu HH, Ho CW, Ko MT and Lin CY: cytoHubba: Identifying hub objects and sub-networks from complex interactome. BMC Syst Biol 8 (Suppl 4): S11, 2014.
25. Zhou N and Bao J: FerrDb: A manually curated resource for regulators and markers of ferroptosis and ferroptosis-disease associations. Database (Oxford) 2020: baaa021, 2020.
26. Bardou P, Mariette J, Escudié F, Djemiel C and Klopp C: jvenn: An interactive Venn diagram viewer. BMC Bioinformatics 15: 293, 2014.
27. Wu T, Hu E, Xu S, Chen M, Guo P, Dai Z, Feng T, Zhou L, Tang W, Zhan L, *et al*: clusterProfiler 4.0: A universal enrichment tool for interpreting omics data. Innovation (Camb) 2: 100141, 2021.
28. Shen W, Song Z, Zhong X, Huang M, Shen D, Gao P, Qian X, Wang M, Li S, Song X, *et al*: Sangerbox: A comprehensive, interaction-friendly clinical bioinformatics analysis platform. iMeta 1: e36, 2022.
29. Szklarczyk D, Gable AL, Lyon D, Junge A, Wyder S, Huerta-Cepas J, Simonovic M, Doncheva NT, Morris JH, Bork P, *et al*: STRING v11: Protein-protein association networks with increased coverage, supporting functional discovery in genome-wide experimental datasets. Nucleic Acids Res 47: D607-D613, 2019.
30. Shannon P, Markiel A, Ozier O, Baliga NS, Wang JT, Ramage D, Amin N, Schwikowski B and Ideker T: Cytoscape: A software environment for integrated models of biomolecular interaction networks. Genome Res 13: 2498-2504, 2003.
31. Wen L, Cheng X, Fan Q, Chen Z, Luo Z, Xu T, He M and He H: TanshinoneIIA inhibits excessive autophagy and protects myocardium against ischemia/reperfusion injury via 14-3-3η/Akt/Beclin1 pathway. Eur J Pharmacol 954: 175865, 2023.
32. HuT, Zou HX, Le SY, Wang YR, Qiao YM, Yuan Y, Liu JC, Lai SQ and Huang H: Tanshinone IIA confers protection against myocardial ischemia/reperfusion injury by inhibiting ferroptosis and apoptosis via VDAC1. Int J Mol Med 52: 109, 2023.
33. Livak KJ and Schmittgen TD: Analysis of relative gene expression data using real-time quantitative PCR and the 2(-Delta Delta C(T)) method. Methods 25: 402-408, 2001.
34. Yoo M, Shin J, Kim J, Ryall KA, Lee K, Lee S, Jeon M, Kang J and Tan AC: DSigDB: Drug signatures database for gene set analysis. Bioinformatics 31: 3069-3071, 2015.
35. Wishart DS, Feunang YD, Guo AC, Lo EJ, Marcu A, Grant JR, Sajed T, Johnson D, Li C, Sayeeda Z, *et al*: DrugBank 5.0: A major update to the DrugBank database for 2018. Nucleic Acids Res 46: D1074-D1082, 2018.
36. Zou HX, Hu T, Zhao JY, Qiu BQ, Zou CC, Xu QR, Liu JC, Lai SQ and Huang H: Exploring Dysregulated ferroptosis-related genes in septic myocardial injury based on human heart transcriptomes: Evidence and new insights. J Inflamm Res 16: 995-1015, 2023.
37. Liu K, Chen S and Lu R: Identification of important genes related to ferroptosis and hypoxia in acute myocardial infarction based on WGCNA. Bioengineered 12: 7950-7963, 2021.
38. Wang Q, Liu B, Wang Y, Bai B, Yu T and Chu XM: The biomarkers of key miRNAs and target genes associated with acute myocardial infarction. PeerJ 8: e9129, 2020.
39. Tarasco M, Gavaia PJ, Bensimon-Brito A, Cardeira-da-Silva J, Ramkumar S, Cordelières FP, Günther S, Bebianno MJ, Stainier DYR, Cancela ML and Laizé V: New insights into benzo[α]pyrene osteotoxicity in zebrafish. Ecotoxicol Environ Saf 226: 112838, 2021.
40. Alissa EM and Ferns GA: Heavy metal poisoning and cardiovascular disease. J Toxicol 2011: 870125, 2011.
41. Wu X, Li Y, Zhang S and Zhou X: Ferroptosis as a novel therapeutic target for cardiovascular disease. Theranostics 11: 3052-3059, 2021.
42. Del Re DP, Amgalan D, Linkermann A, Liu Q and Kitsis RN: Fundamental mechanisms of regulated cell death and implications for heart disease. Physiol Rev 99: 1765-1817, 2019.
43. Fang X, Ardehali H, Min J and Wang F: The molecular and metabolic landscape of iron and ferroptosis in cardiovascular disease. Nat Rev Cardiol 20: 7-23, 2023.
44. Feng Y, Madungwe NB, Imam Aliagan AD, Tombo N and Bopassa JC: Liproxstatin-1 protects the mouse myocardium against ischemia/reperfusion injury by decreasing VDAC1 levels and restoring GPX4 levels. Biochem Biophys Res Commun 520: 606-611, 2019.
45. Li W, Li W, Leng Y, Xiong Y and Xia Z: Ferroptosis is involved in diabetes myocardial ischemia/reperfusion injury through endoplasmic reticulum stress. DNA Cell Biol 39: 210-225, 2020.
46. Baba Y, Higa JK, Shimada BK, Horiuchi KM, Suhara T, Kobayashi M, Woo JD, Aoyagi H, Marh KS, Kitaoka H and Matsui T: Protective effects of the mechanistic target of rapamycin against excess iron and ferroptosis in cardiomyocytes. Am J Physiol Heart Circ Physiol 314: H659-H668, 2018.
47. Andrews NC: Forging a field: The golden age of iron biology. Blood 112: 219-230, 2008.
48. Gao G, Li J, Zhang Y and Chang YZ: Cellular Iron Metabolism and Regulation. Adv Exp Med Biol 1173: 21-32, 2019.
49. Paterek A, Mackiewicz U and Mączewski M: Iron and the heart: A paradigm shift from systemic to cardiomyocyte abnormalities. J Cell Physiol 234: 21613-21629, 2019.
50. Zhang QJ, He Y, Li Y, Shen H, Lin L, Zhu M, Wang Z, Luo X, Hill JA, Cao D, *et al*: Matricellular protein cilp1 promotes myocardial fibrosis in response to myocardial infarction. Circ Res 129: 1021-1035, 2021.
51. Schroer AK, Bersi MR, Clark CR, Zhang Q, Sanders LH, Hatzopoulos AK, Force TL, Majka SM, Lal H and Merryman WD: Cadherin-11 blockade reduces inflammation-driven fibrotic remodeling and improves outcomes after myocardial infarction. JCI Insight 4: e131545, 2019.
52. Snider JC, Riley LA, Mallory NT, Litsky AS, Stoodley P, Swinehart SD, Duerr RA, Kaeding CC and Flanigan DC: Targeting 5-HT2B receptor signaling prevents border zone expansion and improves microstructural remodeling after myocardial infarction. Circulation 143: 1317-1330, 2021.
53. Humeres C and Frangogiannis NG: Fibroblasts in the Infarcted, remodeling, and failing heart. JACC Basic Transl Sci 4: 449-467, 2019.
54. Talman V and Ruskoaho H: Cardiac fibrosis in myocardial infarction-from repair and remodeling to regeneration. Cell Tissue Res 365: 563-581, 2016.
55. Chen Y, Li X, Wang S, Miao R and Zhong J: Targeting iron metabolism and ferroptosis as novel therapeutic approaches in cardiovascular diseases. Nutrients 15: 59, 2023.
56. Angelova PR, Choi ML, Berezhnov AV, Horrocks MH, Hughes CD, De S, Rodrigues M, Yapom R, Little D, Dolt KS, *et al*: Alpha synuclein aggregation drives ferroptosis: An interplay of iron, calcium and lipid peroxidation. Cell Death Differ 27: 2781-2796, 2020.
57. Yu M, Lin Z, Tian X, Chen S, Liang X, Qin M, Zhu Q, Wu Y and Zhong S: Downregulation of Cx43 reduces cisplatin-induced acute renal injury by inhibiting ferroptosis. Food Chem Toxicol 158: 112672, 2021.
58. Huang Q, Sha W, Gu Q, Wang J, Zhu Y, Xu T, Xu Z, Yan F, Lin X and Tian S: Inhibition of Connexin43 improves the recovery of spinal cord injury against ferroptosis via the SLC7A11/GPX4 pathway. Neuroscience 526: 121-134, 2023.
59. Beutler E, Barton JC, Felitti VJ, Gelbart T, West C, Lee PL, Waalen J and Vulpe C: Ferroportin 1 (SCL40A1) variant associated with iron overload in African-Americans. Blood Cells Mol Dis 31: 305-309, 2003.
60. Wiggert B, Bergsma DR, Helmsen R and Chader GJ: Vitamin A receptors. Retinoic acid binding in ocular tissues. Biochem J 169: 87-94, 1978.
61. Choudhary R, Baker KM and Pan J: All-trans retinoic acid prevents angiotensin II- and mechanical stretch-induced reactive oxygen species generation and cardiomyocyte apoptosis. J Cell Physiol 215: 172-181, 2008.
62. Lou S, Zhong L, Yang X, Xue T, Gai R, Zhu D, Zhao Y, Yang B, Ying M and He Q: Efficacy of all-trans retinoid acid in preventing nickel induced cardiotoxicity in myocardial cells of rats. Food Chem Toxicol 51: 251-258, 2013.
63. Nizamutdinova IT, Guleria RS, Singh AB, Kendall JA, Baker KM and Pan J: Retinoic acid protects cardiomyocytes from high glucose-induced apoptosis through inhibition of NF-κB signaling pathway. J Cell Physiol 228: 380-392, 2013.

64. Yamaguchi A, Uchida M, Ishibashi H, Hirano M, Ichikawa N, Arizono K, Koyama J and Tominaga N: Potential mechanisms underlying embryonic developmental toxicity caused by benzo[a] pyrene in Japanese medaka (Oryzias latipes). Chemosphere 242: 125243, 2020.
65. Feng B, Li L, Xu H, Wang T, Wu R, Chen J, Zhang Y, Liu S, Ho SSH, Cao J and Huang W: PM2.5-bound polycyclic aromatic hydrocarbons (PAHs) in Beijing: Seasonal variations, sources, and risk assessment. J Environ Sci (China) 77: 11-19, 2019.
66. Wu Y, Huang T, Li X, Shen C, Ren H, Wang H, Wu T, Fu X, Deng S, Feng Z, *et al*: Retinol dehydrogenase 10 reduction mediated retinol metabolism disorder promotes diabetic cardiomyopathy in male mice. Nat Commun 14: 1181, 2023.